 E-ISSN: 2303-0720

DOI: https://doi.org/10.21009/JRSKT.121.04

Coupled Raman and FTIR Analysis of Biomass-Derived Carbon Prepared at Low Carbonization Temperature

Gugus Handika[1], Fairuz Gianirfan Nugroho[2], Afina Faza Hafiyyan[1], Feber Valentin Br Sembiring[3], Neysa Azzahra[4], Didik Aryanto[5], Abu Saad Ansari[1,6,*a)], Nurul Taufiqu Rochman[7,*b)]

[1]*Center of Excellence Applied Nanotechnology, Nano Center Indonesia, Puspiptek, South Tangerang, Banten 15314, Indonesia*
[2]*Department of Chemistry, Faculty of Mathematics and Natural Sciences, Universitas Negeri Jakarta, Rawamangun, Jakarta Timur, DKI Jakarta 13220*
[3]*Bachelor's Program in Physical Engineering, Institut Teknologi Sumatera, Lampung Selatan, Lampung 35365, Indonesia*
[4]*Bachelor's Program in Chemistry, IPB University, Bogor, West Java 16680, Indonesia*
[5]*Research Center for Energy Materials, National Research and Innovation Agency, KST BJ. Habibie, Serpong, Kota, Tangerang, Selatan, Banten, 15314, Indonesia*
[6]*Global Research and Development and Innovation Center, Nano Center Indonesia, Puspiptek, South Tangerang, Banten 15314, Indonesia*
[7]*Research Center for Advanced Material, National Research and Innovation Agency (BRIN), Puspiptek, South Tangerang, Banten 15314, Indonesia*

*Email: [a)]saad@nano.or.id; [b)]nurul@nano.or.id

Received: 27 January 2026
Revised: 28 February 2026
Accepted: 29 May 2026
Online: 24 June 2026
Published: 30 June 2026

Jurnal Riset Sains dan Kimia Terapan
p-ISSN: 2302 - 8467
e-ISSN: 2303 – 0720

Abstract

Biomass-derived carbon is commonly produced at high temperatures to promote graphitization; however, understanding carbon formation at lower temperatures remains critical for applications that rely on surface reactivity rather than crystallinity. In this work, carbon obtained from oil palm empty fruit bunch (EFB) through pyrolysis at 500 °C was systematically investigated using coupled Fourier transform infrared (FTIR) and Raman spectroscopy, supported by density functional theory (DFT)-based structural interpretation. FTIR analysis reveals extensive dehydration, cleavage of aliphatic C–H bonds, and progressive loss of oxygenated functional groups, accompanied by the emergence of aromatic C=C and C–O–C linkages. Raman spectra, resolved through pseudo-Voigt deconvolution, are dominated by defect-related bands (D, D_2, D_3, and D_4) with a broadened G band, indicating the formation of small, disordered sp^2 carbon domains rather than extended graphitic lattices. DFT-assisted analysis suggests that the carbon framework is composed of interconnected polyaromatic hydrocarbon clusters incorporating residual heteroatoms and mixed sp^2–sp^3 bonding. These results demonstrate that low-temperature pyrolysis of EFB produces a defect-rich aromatic carbon structure strongly governed by precursor chemistry, offering a viable route for tailoring functional carbon materials with abundant active sites, making it highly suitable for applications in adsorption, catalysis, and environmental remediation technologies.

Keywords: Biochar, Empty Fruit Bunch (EFB), FTIR, Pyrolysis, Raman

 E-ISSN: 2303-0720

Introduction

The increasing demand for sustainable and high-performance carbon materials has driven significant interest in biomass-derived carbons as renewable alternatives to diverse applications in many industries (Ansari et al., 2025). Biomass offers a unique advantage as a carbon source due to its abundance, low cost, and intrinsic chemical diversity, which enables the tailoring of carbon structures through controlled thermochemical conversion processes (Zhou & Wang, 2020). The physicochemical properties of the resulting carbon, such as hybridization state, defect density, and surface functionality, are strongly influenced by both the nature of the biomass precursor and the conditions employed during carbonization (Li et al., 2021). The pyrolysis method has emerged as an effective route for producing biochar with tunable physicochemical properties, ranging from amorphous carbon to partially ordered aromatic and graphitic domains (Nugroho et al., 2024; M. Zhang et al., 2022). High-temperature carbonization is often employed to promote graphitization and long-range ordering, while low-temperature pyrolysis is commonly employed as a controlled thermochemical route to convert lignocellulosic biomass into carbon-rich solids while preserving a significant portion of the original chemical functionality (Putri et al., 2026). This process limits extensive graphitization and instead promotes partial carbonization. The presence of the remaining functional groups on the carbon surface is advantageous for applications that rely on surface reactivity rather than high crystallinity, including adsorption, catalysis, and interfacial reaction (Ahmed et al., 2022). However, the structural evolution of biomass-derived carbon at early stages of carbonization remains insufficiently understood, especially at temperatures around 500 °C, where amorphization and char formation are initially observed, and structural ordering coexists with chemical transformation (Janu et al., 2021; Lu & Gu, 2022).

Understanding carbon formation at low temperatures requires analytical techniques capable of probing both chemical bonding and carbon lattice structure. Fourier transform infrared (FTIR) spectroscopy is highly sensitive to functional groups and provides direct evidence of bond cleavage, dehydration, and deoxygenation during biomass decomposition (Munajad et al., 2018; Yang et al., 2019). In contrast, Raman spectroscopy provides insight into carbon hybridization, defect density, and aromatic ordering (Puech et al., 2019). When used in a complementary manner, these analytical techniques offer a comprehensive understanding of how chemical reactions and structural rearrangements proceed during low-temperature pyrolysis (Brubaker et al., 2021). (EFB) represents an abundant lignocellulosic waste generated by the palm oil industry, with annual production reaching ~28.65 million tons globally (Yulistiani et al., 2025). Despite its abundance, EFB is underutilized and can cause environmental issues; its conversion into functional carbon materials offers both environmental and technological benefits. Rich in cellulose (~37%), hemicellulose (~31.5%), and lignin (~31.5%), EFB provides a chemically complex precursor that is well-suited for investigating biomass-to-carbon transformation pathways (Kostryukov et al., 2023). These three components play a critical role in influencing the graphitic structure of biochar (Chiang et al., 2023). It is observed that the trace of hemicellulose affects the physical structure of biochar, while higher lignin content may disrupt the degree of carbonization. Therefore, extracting cellulose-rich fractions has been pursued to achieve higher yields of graphene oxide. Further, some studies used them to achieve the expected functionalization of the biochar in specific applications (Hoang et al., 2020; Khanna et al., 2017; Reza Arrafi et al., 2019).

In this study, we investigate the formation of biomass-derived carbon from EFB through controlled pyrolysis at 500 °C. In biomass carbonization processes, 500 °C is generally considered low because it is lower than the temperature required to achieve substantial graphitization and long-range structural ordering, which typically develops at or above 700 °C. By employing coupled FTIR and Raman spectroscopy, we elucidate the relationship between functional group evolution, defect formation, and aromatic domain development. This work provides mechanistic insight into low-temperature carbonization of lignocellulosic biomass and highlights the critical role of precursor chemistry in governing the structure of defect-rich carbon materials.

 E-ISSN: 2303-0720

Method

Oil palm EFB in fibrous form was bought from a local supplier in the Banten region, Indonesia. The EFB fibers were first thoroughly rinsed with deionized water to remove dirt, dust, and contaminants. The cleaned fibers were then dried in an oven at 100°C for 12 h to remove moisture and volatiles that could disrupt the pyrolysis process. After drying, the fibers were crushed into powder through disc milling for 2 minutes to obtain a homogeneous and fine powder. Then, the powder was sieved through a 325 mesh. Pyrolysis of EFB powder was performed in a furnace at 500 °C for 1 h under an inert atmosphere with a heating rate of 3 °C/min, consistent with our previous research study (Nugroho et al., 2024). Briefly, powder was kept in an alumina crucible, thereafter a slight flame was introduced to remove oxygen, followed by immediate closing of the crucible and heating in a furnace. After natural cooling to room temperature (RT), the resulting solid residues were collected and designated as biomass-derived carbon (biochar).

FTIR spectra were recorded using a Thermo Scientific Nicolet iS10 equipped with a diamond attenuated total reflectance (ATR) accessory. All spectra were taken over the spectral range of 400 – 4000 cm^{-1} with a spectral resolution of 4 cm^{-1}. Raman spectroscopy analysis was taken with Thermo Scientific DXR2xi Raman Microscope Spectroscopy equipped with a 532 nm laser and 50× objective lens. The laser power was set to 5 mW to avoid local heating effects. Each spectrum was acquired using an exposure time of 250 ms and accumulated over 200 scans to improve the signal-to-noise ratio. The possible structures present after pyrolysis are built using Avagadro software.

Results and Discussion

The effect of pyrolysis temperature on biochar.

Figure 1 shows the FTIR spectra of EFB and the carbonized sample obtained at 500 °C, providing direct insight into the chemical evolution of the biomass during low-temperature pyrolysis. The FTIR profile of untreated EFB is consistent with those commonly reported for lignocellulosic biomass, confirming that EFB is mainly composed of cellulose, hemicellulose, and lignin (Kostryukov et al., 2023).

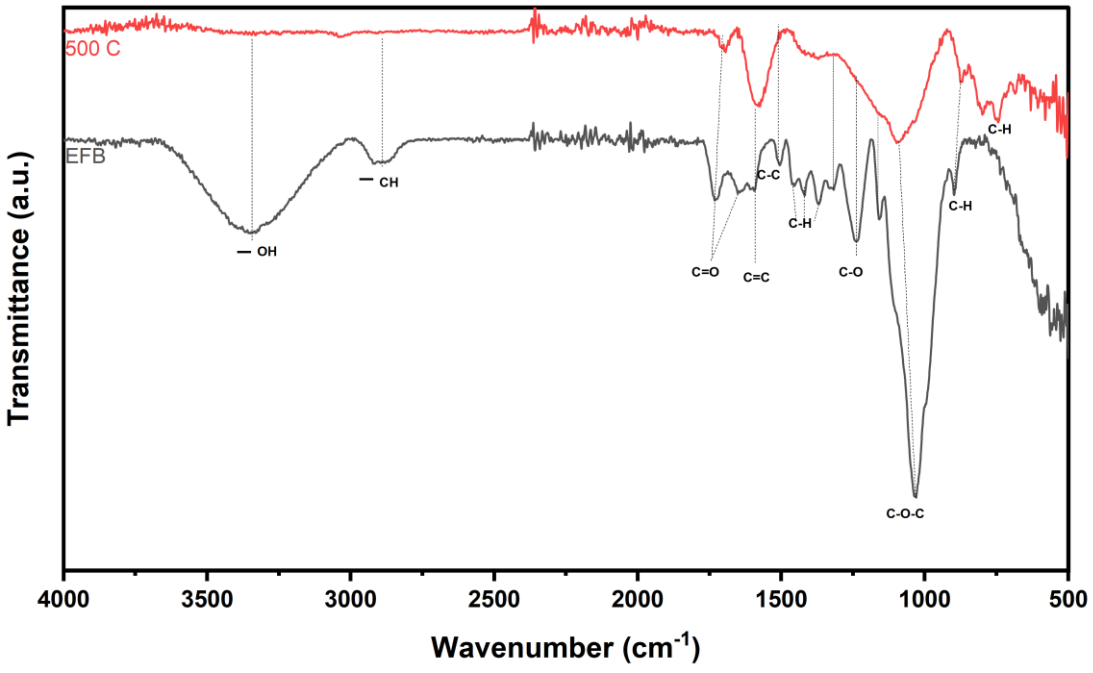

Figure 1. Fourier transform infrared spectroscopy (FTIR) spectra of empty fruit bunch and its pyrolyzed state

 E-ISSN: 2303-0720

In the EFB spectrum, the broad absorption centered around 3300–3400 cm^{-1} corresponds to O–H stretching vibrations arising from hydroxyl groups in cellulose and hemicellulose, as well as phenolic moieties in lignin (Kacuráková, 2000). The band in the 2850–2950 cm^{-1} region is attributed to C–H stretching of methyl and methylene groups associated with carbohydrate chains (Lani et al., 2014). The hemicellulose presence is evidenced by carbonyl-related absorptions near 1728 cm^{-1} and 1652 cm^{-1}, originating from acetyl and uronic ester groups that are absent in pure cellulose (Apaydın Varol & Mutlu, 2023). In the fingerprint region 800–1400 cm^{-1}, multiple bands associated with C–O, C–C, and C–H vibrations depict the glycosidic linkages and ring structures of polysaccharides (Kostryukov et al., 2023). Lignin exhibits a more complex spectrum due to its aromatic nature, consisting of guaiacyl and syringyl units with strong C=C, C–C, and C–O–C stretching vibrations (M. Zhang et al., 2022). The detailed band assignments are summarized in **Table 1**.

Table 1. FTIR Spectra and Band Assignment of Empty Fruit Bunch

EFB (cm^{-1})	500 °C (cm^{-1})	Vibrational Modes	References
3342	-	O–H stretching vibrations	(Kostryukov et al., 2023)
2882	-	Symmetric and asymmetric C–H vibrations in CH, CH_2, and CH_3	(Kostryukov et al., 2023)
1728	-	C=O stretching vibrations carbonyl and carboxyl (hemicellulose)	(Kostryukov et al., 2023; Lani et al., 2014; Zakaria & Liew, 2013)
-	1694	C=O stretching vibrations in phenolic ester	(Kostryukov et al., 2023; Lani et al., 2014; Zakaria & Liew, 2013)
1652	-	C=O stretching vibrations in p-ketones (hemicellulose)	(Kostryukov et al., 2023; Lani et al., 2014; Zakaria & Liew, 2013)
1597	1574	C=C asymmetric stretching of alkene in aromatic rings, condensed (lignin)	(Kostryukov et al., 2023)
1505	1574	C–C skeletal vibrations in aromatic rings (lignin)	(Kostryukov et al., 2023)
1455	1455	Asymmetric bending vibrations of CH, CH_2, and CH_3	(Kostryukov et al., 2023)
1418	1418	Symmetric bending vibration of CH_2 groups	(Kostryukov et al., 2023)
1372	1371	O–H in plane bending vibrations of phenol (lignin); O–H in plane bending vibrations (cellulose and hemicellulose)	(Kostryukov et al., 2023)
1318	1318	Skeletal vibrations of the syringyl and condensed guaiacyl ring (lignin); C–H bending vibrations (hemicellulose and cellulose)	(Kostryukov et al., 2023)
1238	1238	Stretching asymmetric vibrations C_{Ar}–O–C (lignin) C–O stretching vibrations in phenols (lignin);	(Kostryukov et al., 2023)
1160	1160	C–O stretching vibrations (lignin); C–O–C glycosidic linkage stretching vibrations (hemicellulose and cellulose)	(Kacuráková, 2000; Kostryukov et al., 2023)
1031	1098	C–O stretching of alcohol groups; symmetric and asymmetric C–O–C bending vibrations	(Kostryukov et al., 2023)
898	872	β anomer of a typical glycosidic linkage	(Kacuráková, 2000; Kostryukov et al., 2023)
-	796	Out of plane C–H bending vibrations of the aromatic rings	(Kostryukov et al., 2023)
-	744	Out of plane C–H bending vibrations of the aromatic rings	(Kostryukov et al., 2023)

 E-ISSN: 2303-0720

After pyrolysis, the FTIR bands associated with the original biomass functional groups decrease in intensity or disappear entirely, reflecting significant chemical restructuring. The O–H and C–H single-bond vibrations vanish completely, demonstrating effective dehydration and cleavage of alkyl side chains, while other oxygen-containing bands are substantially reduced. This spectral evolution indicates the onset of bond cleavage and condensation reactions, which promote the formation of larger and more stable aromatic domains (Apaydın Varol & Mutlu, 2023). During this process, cellulose decomposes through the breakdown of its glucopyranose backbone, whereas hemicellulose undergoes partial degradation, retaining carbonyl (C=O) functionalities at acetyl sites, as evidenced by the band at 1696 cm^{-1} (Barszcz et al., 2024). This transformation is further supported by the shift and reduction of the C–O–C stretching band from 1031 cm^{-1} to a new peak at 1098 cm^{-1}, signifying glucose depolymerization. Additionally, alkyl-related vibrations in the 1300–1400 cm^{-1} region undergo bond scission, resulting in the emergence of new peaks at 796 cm^{-1} and 744 cm^{-1}, which are characteristic of out-of-plane C–H bending modes in aromatic rings. Lignin, as the most thermally stable constituent, persists throughout pyrolysis and becomes the dominant structural component of the resulting biochar, as indicated by strong aromatic C=C stretching at 1574 cm^{-1} and aryl–ether (C_{Ar}–O–C) vibrations at 1238 cm^{-1} (Lu & Gu, 2022).

Defect-Dominated sp^2 Carbon Formation.

Raman spectroscopy was employed to elucidate the structural ordering, hybridization state, and defect characteristics of the carbon produced from EFB at a carbonization temperature of 500 °C. The Raman spectrum exhibits broad and overlapping features, which were deconvoluted using a pseudo-Voigt function, a widely adopted approach for resolving overlapping bands commonly observed in disordered carbonaceous materials (Tagliaferro et al., 2020). **Figure 2** depicts the deconvoluted Raman spectrum of EFB-derived carbon obtained at 500 °C. Two dominant peaks are observed centered near 1350 cm^{-1} and 1580 cm^{-1}, commonly referred to as the D ("disorder") and G ("graphitic") bands, respectively, accompanied by minor shoulder bands. The G band originates from the in-plane E_{2g} vibrational mode of sp^2-bonded carbon atoms, and is indicative of aromatic ring stretching within graphitic or graphitic-like domains (Puech et al., 2019), while the D band arises from structural defects associated with disrupted C–C bonding and condensed aromatic ring imperfections (P. Zhang et al., 2024).

As evident from the spectrum, the D-band intensity is higher than that of the G band, and both bands appear relatively broad. This spectral signature reflects a carbon framework dominated by defects, edge sites, and small aromatic clusters rather than extended graphitic crystallites. Such behavior is characteristic of the early stages of pyrolysis, during which reactions such as depolymerization, dehydration, side-chain scission, demethoxylation, and carbohydrate fragmentation generate a high density of structural defects, including vacancies, edge sites, grain boundaries, and heteroatom incorporation within the carbon lattice (Lu & Gu, 2022). Beyond the primary D and G bands, several defect-related sub-bands are observed. The D_3 band, located at approximately 1492 cm^{-1}, is associated with amorphous carbon contributions and is commonly attributed to vibrational modes of disordered polyaromatic structures and non-hexagonal ring systems (C. C. Zhang et al., 2022), caused by the restructuring of C–H bonds within aromatic systems, particularly the stretching and bending of methyl and methylene groups, which disrupts ring symmetry. The presence of a pronounced D_3 band suggests incomplete carbonization and the coexistence of amorphous carbon regions alongside emerging aromatic domains, consistent with the partial retention of oxygenated functionalities observed in the FTIR analysis. The D_4 band, appearing near 1200 cm^{-1}, corresponds to mixed sp^2–sp^3 carbon configurations within aromatic structures and is particularly associated with aryl–alkyl linkages (para-substituted aromatics) and aromatic–aliphatic ether bonds (Xu et al., 2018). This band reflects the structural inheritance from the lignocellulosic precursor, where aromatic units are interconnected by residual aliphatic bridges. The persistence of such bonding motifs indicates that carbonization at 500 °C likely retains some sp^3 carbon while producing a heterogeneous carbon network. The D_2 band, which tends to be overlapped by the G band, is attributed to surface-related defects and graphitic lattice distortions analogous to the E_2g symmetry of the G band, which is currently negligible in the fabricated biochar (P. Zhang et al., 2024). This extension feature is linked to the carbonyl (C=O) group that perturbs the symmetry of sp^2 domains, a phenomenon frequently observed in graphite oxide and

 E-ISSN: 2303-0720

partially reduced carbon materials (Gao et al., 2009). The presence of the D_2 feature supports the argument that the carbon structure retains chemically active defect sites at this stage of thermal treatment.

The peak area band ratios were used to approximate the oxygen/carbon ratio in the structure (inset **Figure 2**). This ratio governs the structural order, amorphicity, and reactive sites of the biochar. The higher ID/IG ratio of 1.14 indicates structural disorder in graphitic carbon. Such a high value represents the elevated defect density, including complex graphitic stacking, low aromatic cluster, and abundant functional groups arising from incomplete thermal decomposition of precursor (Li et al., 2023). Meanwhile, this ratio contributes to the graphitic stability of biochar, as evidenced by Sheng et al. (Sheng, 2007), where demineralized coal is less reactive than its previous mineral-rich counterpart. Recent work further supports this, where oxygen content alters the graphitic structure of coal, probing the functionalization on the way during graphitization described by the I_G/I_{D3+D4} ratio. (S. Zhang et al., 2024). The additional D_3 and D_4 related to the specialization of functional groups derived from the With $I_G/I_{D3+D4} = 0.7$ (less than 1), along with I_G/I_{all} of 0.35, the biochar possesses a high reactivity due to high functionalization groups, and less stable graphitic order. The $FWHM_G$ also plays a crucial role in assessing the structural evolution of biochar, as a complement to I_D/I_G analysis (Cancado et al., 2011). The G band FWHM of the fabricated biochar is 115 cm^{-1}, indicating complex heterogeneity in defect types, i.e., edges, holes, substitutional atoms, grain boundaries, and cracks.

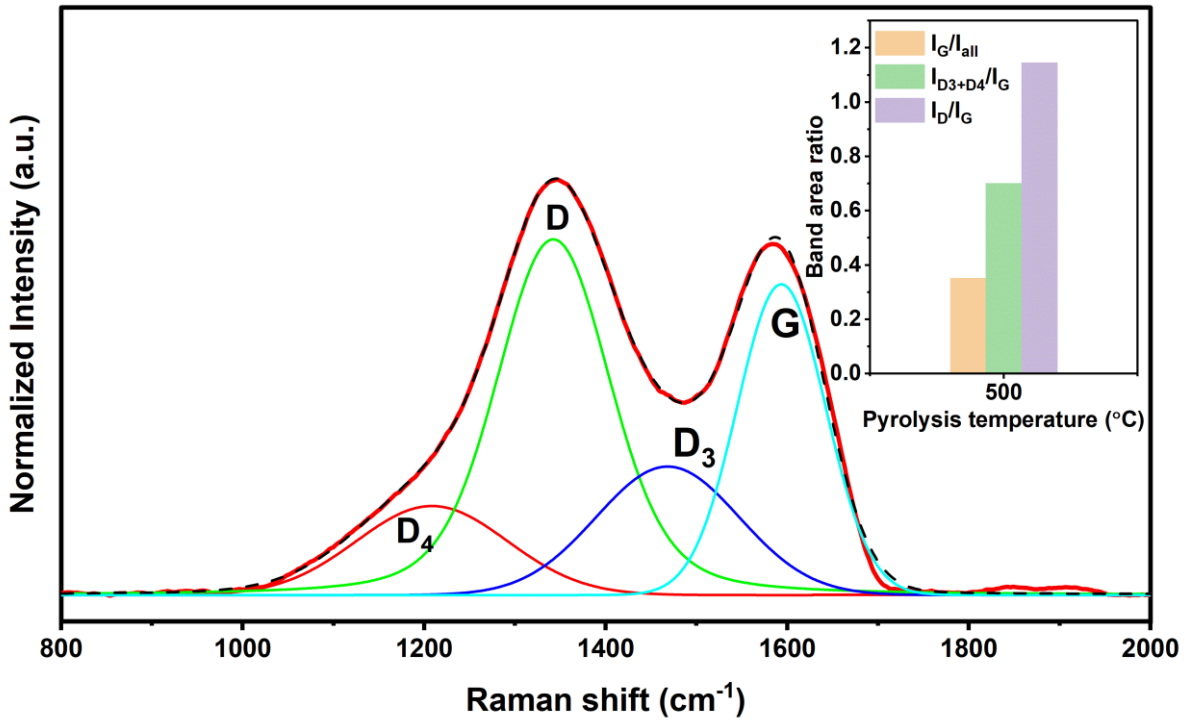

Figure 2. Pyrolytic Raman Spectra of Empty Fruit Bunch at 500°C Fitted Into 4 Bands with Inset Figure of Area Band Ratio

Overall, the Raman spectral features indicate that carbonization of EFB at 500 °C yields a defect-rich, aromatic carbon framework composed of small polyaromatic units interconnected through disordered bonding motifs. The dominance of defect-related bands over the graphitic G band confirms that the carbon structure is governed by the chemical nature of the biomass precursor rather than by thermally driven graphitization. These findings align with previous studies on biomass-derived carbons, which emphasize that low-temperature pyrolysis favors the formation of structurally heterogeneous carbon with high defect density and limited crystallinity (Smith et al., 2016).

To rationalize the spectroscopic features observed in the FTIR and Raman analyses, a molecular-level structural model is proposed for the carbon produced from EFB at 500 °C, as seen in **Figure 3**. At this relatively low carbonization temperature, the carbon framework cannot be described as

 E-ISSN: 2303-0720

graphitic; instead, it consists of a heterogeneous assembly of small polyaromatic hydrocarbon (PAH) units interconnected through defective and oxygen-containing linkages. Such structural complexity is a characteristic feature of biomass-derived carbon formed during early-stage pyrolysis, where chemical inheritance from the precursor plays a dominant role (Smith et al., 2016). Density functional theory (DFT) calculations reported in the literature provide valuable insight into how specific molecular motifs contribute to Raman-active vibrational modes in disordered carbon systems. It demonstrated that the D band originates from breathing modes of small aromatic clusters, including naphthalene-, pyrene-, and perylene-like structures, which are activated by structural disorder and finite crystallite size (Smith et al., 2016). The D_3 band observed near 1490 cm^{-1} is attributed to amorphous vibrational modes associated with irregular PAH arrangements and non-ideal ring configurations. DFT-based analyses have shown that vibrations from distorted aromatic systems, including fused rings with heteroatom substitution or edge hydrogenation, contribute strongly to this spectral region (Smith et al., 2016). The shoulder observed in the 1150–1200 cm^{-1} region, associated with the D_4 band, corresponds to vibrational modes of cycloheptane and larger ring structures. Meanwhile, the spectral features of the G band are related to the coupling of breathing modes and asymmetric stretching, arising from strain-induced deformation within PAH systems and constriction motions caused by oxygen incorporation in coronene-based structures. The low-temperature carbonization of EFB produces a chemically complex carbon framework similar to a benzo(a)pyrene structure with oxygenated defects inside the aromatics, according to the peak ratio as discussed earlier. Such defect-rich carbon architectures are particularly relevant for applications requiring high surface reactivity, active sites, and functional group accessibility. It should be noted that this interpretation is based on a single carbonization temperature (500 °C), and a temperature-dependent study would be necessary to fully distinguish the roles of precursor chemistry and thermal effects.

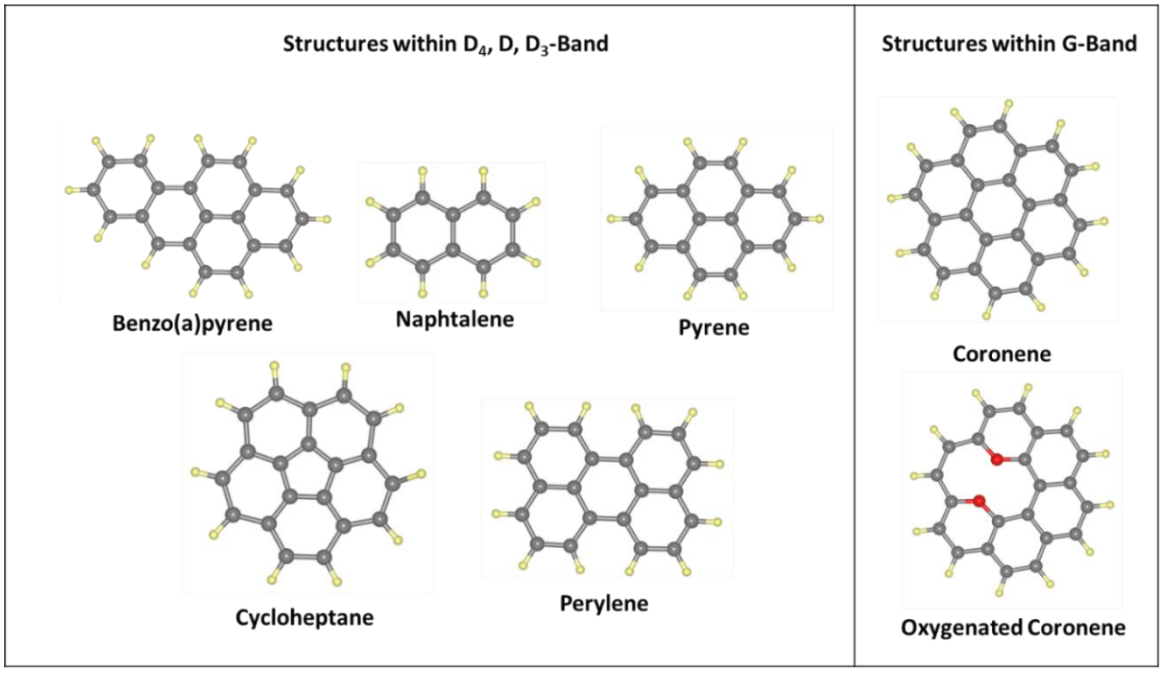

Figure 3. Representative polyaromatic hydrocarbon structures associated with the D4, D, D3, and G Raman bands of biomass-derived carbon carbonized at 500 °C. Yellow, grey, and red spheres represent H, C, and O atoms, respectively.

Conclusion

This study demonstrates that meaningful carbon formation from oil palm empty fruit bunch (EFB) can be achieved at a relatively low carbonization temperature. The coupled use of FTIR and Raman spectroscopy provides a powerful and complementary approach for elucidating the hybridization state

 E-ISSN: 2303-0720

and structural evolution of EFB-derived carbon during pyrolysis. Pyrolysis at 500 °C initiates multiple thermochemical reactions, including depolymerization, dehydration, side-chain scission, demethoxylation, and carbohydrate fragmentation, which collectively drive the transformation of the native lignocellulosic structure into an aromatic carbon framework. FTIR analysis reveals the effective elimination of O–H and C–H single bonds, accompanied by progressive aromatization and the formation of stronger C=C, C–C, and C–O–C linkages. Raman spectroscopy further clarifies this transformation by resolving defect-related features (D, D_2, D_3, and D_4 bands) associated with aromatic side-chain substitutions, ether linkages, and mixed sp^2–sp^3 hybridization. These defect structures induce lattice deformation, amorphization, and surface vacancies, reflecting the incomplete ordering characteristic of early-stage carbonization. Collectively, the results indicate that the carbon structure formed at this stage is highly defect-rich and strongly influenced by the chemical nature of the biomass precursor, highlighting the critical role of controlled pyrolysis in tailoring biomass-derived carbon allotropes.

Acknowledgments

The authors gratefully acknowledge the financial support for this study provided by New Energy and Industrial Technology Development Organisation (NEDO) in Japan, in collaboration with the National Research and Innovation Agency in Indonesia, according to the Decree of the Deputy for Research and Innovation Facilitation of the National Research and Innovation Agency No. 60/II.7/HK/202.

References

Ahmed, A. T. A., Soni, R., Ansari, A. S., Lee, C. Y., Kim, H.-S., Im, H., & Bathula, C. (2022). Biowaste-derived graphitic carbon interfaced TiO2 as anode for lithium-ion battery. *Surfaces and Interfaces*, *35*, 102404. https://doi.org/https://doi.org/10.1016/j.surfin.2022.102404

Ansari, A. S., Azzahra, G., Nugroho, F. G., Mujtaba, M. M., & Ahmed, A. T. A. (2025). Oxides and Metal Oxide/Carbon Hybrid Materials for Efficient Photocatalytic Organic Pollutant Removal. *15*(2), 134. https://doi.org/10.3390/catal15020134

Apaydın Varol, E., & Mutlu, Ü. (2023). TGA-FTIR Analysis of Biomass Samples Based on the Thermal Decomposition Behavior of Hemicellulose, Cellulose, and Lignin. *Energies*, *16*(9). https://doi.org/10.3390/en16093674

Barszcz, W., Lozynska, M., & Molenda, J. (2024). Impact of pyrolysis process conditions on the structure of biochar obtained from apple waste. *Sci Rep*, *14*(1), 10501. https://doi.org/10.1038/s41598-024-61394-8

Brubaker, Z. E., Langford, J. J., Kapsimalis, R. J., & Niedziela, J. L. (2021). Quantitative analysis of Raman spectral parameters for carbon fibers: practical considerations and connection to mechanical properties. *Journal of Materials Science*, *56*(27), 15087-15121. https://doi.org/10.1007/s10853-021-06225-1

Cancado, L. G., Jorio, A., Ferreira, E. H., Stavale, F., Achete, C. A., Capaz, R. B.,…Ferrari, A. C. (2011). Quantifying defects in graphene via Raman spectroscopy at different excitation energies. *Nano Lett*, *11*(8), 3190-3196. https://doi.org/10.1021/nl201432g

Chiang, A. K. M., Ng, L. Y., Ng, C. Y., Lim, Y. P., Mahmoudi, E., Tan, L. S., & Mah, S. K. (2023). Conversion of palm oil empty fruit bunches to highly stable and fluorescent graphene oxide quantum dots: An eco-friendly approach. *Materials Chemistry and Physics*, *309*. https://doi.org/10.1016/j.matchemphys.2023.128433

Gao, W., Alemany, L. B., Ci, L., & Ajayan, P. M. (2009). New insights into the structure and reduction of graphite oxide. *Nat Chem*, *1*(5), 403-408. https://doi.org/10.1038/nchem.281

Hoang, L. P., Van, H. T., Nguyen, T. T. H., Nguyen, V. Q., Quang Thang, P., & Lee, W. (2020). Coconut Shell Activated Carbon/CoFe2O4 Composite for the Removal of Rhodamine B from Aqueous Solution. *Journal of Chemistry*, *2020*, 1-12. https://doi.org/10.1155/2020/9187960

 E-ISSN: 2303-0720

Janu, R., Mrlik, V., Ribitsch, D., Hofman, J., Sedláček, P., Bielská, L., & Soja, G. (2021). Biochar surface functional groups as affected by biomass feedstock, biochar composition and pyrolysis temperature. *Carbon Resources Conversion*, *4*, 36-46. https://doi.org/10.1016/j.crcon.2021.01.003

Kacuráková, M. (2000). FT-IR study of plant cell wall model compounds: pectic polysaccharides and hemicelluloses. *Carbohydrate Polymers*, *43*(2), 195-203. https://doi.org/10.1016/s0144-8617(00)00151-x

Khanna, R., Ikram-Ul-Haq, M., Rawal, A., Rajarao, R., Sahajwalla, V., Cayumil, R., & Mukherjee, P. S. (2017). Formation of carbyne-like materials during low temperature pyrolysis of lignocellulosic biomass: A natural resource of linear sp carbons. *Sci Rep*, *7*(1), 16832. https://doi.org/10.1038/s41598-017-17240-1

Kostryukov, S. G., Matyakubov, H. B., Masterova, Y. Y., Kozlov, A. S., Pryanichnikova, M. K., Pynenkov, A. A., & Khluchina, N. A. (2023). Determination of Lignin, Cellulose, and Hemicellulose in Plant Materials by FTIR Spectroscopy. *Journal of Analytical Chemistry*, *78*(6), 718-727. https://doi.org/10.1134/s1061934823040093

Lani, N. S., Ngadi, N., Johari, A., Jusoh, M., & Kumar, P. (2014). Isolation, Characterization, and Application of Nanocellulose from Oil Palm Empty Fruit Bunch Fiber as Nanocomposites. *Journal of Nanomaterials*, *2014*(1). https://doi.org/10.1155/2014/702538

Li, Q., Hu, C., Li, M., Truong, P., Li, J., Lin, H.-S.,…Yuan, J. S. (2021). Enhancing the multi-functional properties of renewable lignin carbon fibers via defining the structure–property relationship using different biomass feedstocks. *Green Chemistry*, *23*(10), 3725-3739. https://doi.org/10.1039/d0gc03828h

Li, Z., Deng, L., Kinloch, I. A., & Young, R. J. (2023). Raman spectroscopy of carbon materials and their composites: Graphene, nanotubes and fibres. *Progress in Materials Science*, *135*. https://doi.org/10.1016/j.pmatsci.2023.101089

Lu, X., & Gu, X. (2022). A review on lignin pyrolysis: pyrolytic behavior, mechanism, and relevant upgrading for improving process efficiency. *Biotechnol Biofuels Bioprod*, *15*(1), 106. https://doi.org/10.1186/s13068-022-02203-0

Munajad, A., Subroto, C., & Suwarno. (2018). Fourier Transform Infrared (FTIR) Spectroscopy Analysis of Transformer Paper in Mineral Oil-Paper Composite Insulation under Accelerated Thermal Aging. *Energies*, *11*(2). https://doi.org/10.3390/en11020364

Nugroho, F. G., Ansari, A. S., Rochman, N. T., Khadtare, S. S., Sree, V. G., Shrestha, N. K.,…Ahmed, A. T. A. (2024). Utilizing Indonesian Empty Palm Fruit Bunches: Biochar Synthesis via Temperatures Dependent Pyrolysis. *Nanomaterials (Basel)*, *15*(1). https://doi.org/10.3390/nano15010050

Puech, P., Kandara, M., Paredes, G., Moulin, L., Weiss-Hortala, E., Kundu, A.,…Monthioux, M. (2019). Analyzing the Raman Spectra of Graphenic Carbon Materials from Kerogens to Nanotubes: What Type of Information Can Be Extracted from Defect Bands? *C*, *5*(4). https://doi.org/10.3390/c5040069

Putri, A. M. H., Ramadhoni, B. F., Yuliusman, & Muharam, Y. (2026). Sequential activation-carbonization strategy for engineering porous carbon from tea twigs biomass toward enhanced CO2 capture. *Journal of CO2 Utilization*, *107*. https://doi.org/10.1016/j.jcou.2026.103425

Reza Arrafi, R., Erdawati, E., & Darwis, D. (2019). Pengaruh Penambahan Biokar Sekam Padi Terhadap Penyerapan Gas CO2 (Carbon Dioxide) Dan Kuat Tekan Pada Plester Dinding. *JRSKT - Jurnal Riset Sains dan Kimia Terapan*, *8*(1), 10-22. https://doi.org/10.21009/jrskt.081.02

Sheng, C. (2007). Char structure characterised by Raman spectroscopy and its correlations with combustion reactivity. *Fuel*, *86*(15), 2316-2324. https://doi.org/10.1016/j.fuel.2007.01.029

Smith, M. W., Dallmeyer, I., Johnson, T. J., Brauer, C. S., McEwen, J.-S., Espinal, J. F., & Garcia-Perez, M. (2016). Structural analysis of char by Raman spectroscopy: Improving band assignments through computational calculations from first principles. *Carbon*, *100*, 678-692. https://doi.org/10.1016/j.carbon.2016.01.031

Tagliaferro, A., Rovere, M., Padovano, E., Bartoli, M., & Giorcelli, M. (2020). Introducing the Novel Mixed Gaussian-Lorentzian Lineshape in the Analysis of the Raman Signal of Biochar. *Nanomaterials (Basel)*, *10*(9). https://doi.org/10.3390/nano10091748

 E-ISSN: 2303-0720

Xu, J., Tang, H., Su, S., Liu, J., Xu, K., Qian, K.,…Xiang, J. (2018). A study of the relationships between coal structures and combustion characteristics: The insights from micro-Raman spectroscopy based on 32 kinds of Chinese coals. *Applied Energy*, *212*, 46-56. https://doi.org/10.1016/j.apenergy.2017.11.094

Yang, D.-P., Li, Z., Liu, M., Zhang, X., Chen, Y., Xue, H.,…Luque, R. (2019). Biomass-Derived Carbonaceous Materials: Recent Progress in Synthetic Approaches, Advantages, and Applications. *ACS Sustainable Chemistry & Engineering*, *7*(5), 4564-4585. https://doi.org/10.1021/acssuschemeng.8b06030

Yulistiani, F., Aqsha, & Bindar, Y. (2025). Sustainable biochar from empty fruit bunches: Technological innovations and future perspectives. *Journal of Analytical and Applied Pyrolysis*, *189*. https://doi.org/10.1016/j.jaap.2025.107111

Zakaria, S., & Liew, T. K. (2013). Characterization of Fe2O3/FeOOH Catalyzed Solvolytic Liquefaction of Oil Palm Empty Fruit Bunch (EFB) Products. *Journal of Bioremediation & Biodegradation*, *s4*. https://doi.org/10.4172/2155-6199.S4-001

Zhang, C. C., Hartlaub, S., Petrovic, I., & Yilmaz, B. (2022). Raman Spectroscopy Characterization of Amorphous Coke Generated in Industrial Processes. *ACS Omega*, *7*(3), 2565-2570. https://doi.org/10.1021/acsomega.1c03456

Zhang, M., Zhang, J., Ran, S., Sun, W., & Zhu, Z. (2022). Biomass-Derived sustainable carbon materials in energy conversion and storage applications: Status and opportunities. A mini review. *Electrochemistry Communications*, *138*. https://doi.org/10.1016/j.elecom.2022.107283

Zhang, P., Fan, J., Wang, Y., Dang, Y., Heumann, S., & Ding, Y. (2024). Insights into the role of defects on the Raman spectroscopy of carbon nanotube and biomass-derived carbon. *Carbon*, *222*. https://doi.org/10.1016/j.carbon.2024.118998

Zhang, S., Wang, M., Liang, C., & Zhu, Z. (2024). Experimental Study on the Improvement of Char Physicochemical Properties and Reactivity by Activation Process in CFB. *ACS Omega*, *9*(23), 24500-24512. https://doi.org/10.1021/acsomega.4c00467

Zhou, C., & Wang, Y. (2020). Recent progress in the conversion of biomass wastes into functional materials for value-added applications. *Sci Technol Adv Mater*, *21*(1), 787-804. https://doi.org/10.1080/14686996.2020.1848213